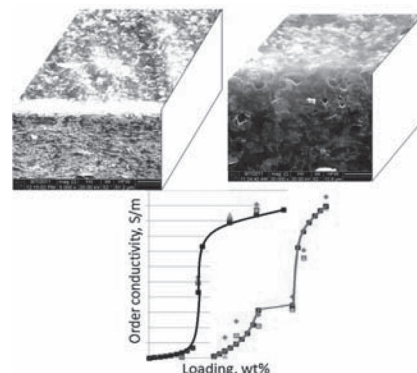


# Graphene Network Organisation in Conductive Polymer Composites

Yuliya V. Syurik, Marcos G. Ghislandi, Evgeniy E. Tkalya, Garry Paterson, Damian McGrouther, Oleg A. Ageev, Joachim Loos\*

A latex technique is used to prepare graphene/polystyrene and graphene/poly(propylene) composites with varying GR loadings. Their electrical properties and the corresponding volume organisation of GR networks are studied. Percolation thresholds for conduction are found to be about 0.9 and 0.4 wt% for GR/PS and GR/PP with maximum obtained conductivities of 12 and 0.4 S m<sup>-1</sup> for GR loadings of 2 wt%, respectively. Investigations using SEM and electrical conductivity measurements show that for the preparation conditions used GR forms an isotropic 3D network in the PS matrix, but GR forms a 2D network in the PP matrix. The different GR network organisations are possibly forced by the different melt flow behaviour of the matrix polymers during processing and the subsequent crystallisation of PP.



## 1. Introduction

Various engineering applications such as antistatics and electromagnetic interference (EMI) shielding require a certain level of conductivity (10<sup>1</sup>–10<sup>7</sup> Ω cm).<sup>[1,2]</sup>

Composites based on polymer matrixes filled with conductive nanoparticles are very promising candidates for production of materials with tuneable electrical conductivity.<sup>[2–5]</sup> The composites can be prepared by incorporation of certain loadings of conductive nanoparticles into the light, cheap and easy processable polymer matrixes. In this respect, an interesting class of conductive nanofillers are carbon allotropes such as carbon black, single- and multi-walled carbon nanotubes (SWCNT and MWCNT), and graphene (GR).<sup>[1,2,4,5]</sup> GR sheets are the one-atom-thick two-dimensional layers of sp<sup>2</sup>-bonded carbon of graphite, best envisioned as an unrolled SWCNT, with a unique combination of mechanical, electrical, and thermal properties and potentially can be produced from very cheap graphite by exfoliation.<sup>[6]</sup>

Preparation of composites filled with nanoparticles having controlled properties still is a challenge. A promising route is application of the latex technique, which allows for straightforward incorporation of predominantly individual nanoparticles into a highly viscous polymer matrix.<sup>[7–10]</sup> For preparing composites filled with GR, a key step of this method is the mixing of an aqueous dispersion of mainly individual GR sheets, covered by surfactant molecules, with colloidal stable polymer latex. In contrast

Yu. V. Syurik, Prof. O. A. Ageev

Taganrog Institute of Technology, Shevchenko Street 2,  
Taganrog 347928, Russia

M. G. Ghislandi

Laboratory of Materials and Interface Chemistry, Eindhoven  
University of Technology, Den Dolech 2, Eindhoven, 5600 MB,  
The Netherlands

E. E. Tkalya

Department of Polymer Chemistry, Eindhoven University  
of Technology, Den Dolech 2, Eindhoven, 5600 MB, The  
Netherlands

Dr. G. Paterson

School of Physics and Astronomy, University of Glasgow,  
University Avenue, Glasgow, G128QQ, United Kingdom

Dr. D. McGrouther, Prof. J. Loos

School of Physics and Astronomy, Kelvin Nanocharacterisation  
Centre and Scottish University Physics Alliance,  
University of Glasgow, University Avenue, Glasgow G128QQ,  
United Kingdom

E-mail: Joachim.Loos@glasgow.ac.uk

with other techniques such as functionalising the nanofiller<sup>[11]</sup> or modifying the polymer matrix,<sup>[12]</sup> the applying latex technique keeps the chemical structure and the functionality of GR intact and almost any kind of polymer matrix can be used, which can be brought into a latex form, that is, amorphous polymer latexes such as polystyrene (PS) or poly(methyl methacrylate), or semicrystalline polymers such as polyethylene or poly(propylene) (PP). Moreover, because of the use of water as dispersant, this technique is environmentally friendly.

Most studies characterising the conductive properties of GR-based composites use conventional 2- or 4-point DC-measurements of composite films for which the probes are brought in contact with the surface of the sample.<sup>[3,13–16]</sup> However, in general, conductive properties have integral character and depend on the volume organisation of the nanoparticle network, which is created in the dielectric polymer matrix. In our study, we have characterised the electrical conductivity behaviour of a series of composites with various GR loadings and different intrinsic properties of their polymer matrixes. Beside conventional 2-point measurements performed exclusively at the top surfaces, we have measured the electrical conductivity through the sample thickness following various conduction paths. Such measurements may be sensitive for nonisotropic GR filler network organisation in the bulk of the samples. Moreover, applying scanning electron microscopy (SEM) charge contrast imaging, we have obtained further information on the volume GR network organisation with high resolution.

## 2. Experimental Section

### 2.1. Samples Preparation

#### 2.1.1. Materials

Semicrystalline PP latex with 29 wt% amount of particles dispersed in water having a  $\overline{M}_w$  below 20 kg mol<sup>-1</sup> (PP, Solvay Priex® 701), poly(styrene sulfonate) with  $\overline{M}_w = 70$  kg mol<sup>-1</sup> (PSS, Aldrich), sodium dodecylsulfate (SDS, Merck), sodium carbonate (SC, Aldrich), and sodium peroxodisulfate (SPS, Merck) were used as received. Styrene (Merck) was purified from an inhibitor at a remover column. Deionised water was used in all reactions. SP-2 graphite (Bay Carbon) was used to prepare the GR nanofiller.

#### 2.1.2. Preparation of PS Latex

In order to obtain PS latex, conventional free radical emulsion polymerisation was carried out in an oxygen-free atmosphere (including prior degassing for 2.5 h with Ar). The reaction was performed at 70 °C with an impeller speed of 400 rpm. In the reactor, 252 g of styrene was mixed with 712 g of water in the presence of 26 g of SDS and 0.7 g of SC buffer. The reaction mixture was degassed for 30 min by purging with argon. A solution of SPS (0.45 g, 1.9 mmol) in H<sub>2</sub>O (10 g) was also degassed. The

polymerisation was initiated by the addition of the initiator solution, and the reaction time was roughly 1 h. The average particle size was 90 nm according to dynamic light scattering, with  $\overline{M}_n$ ,  $\overline{M}_w$  and PDI values of 495 and 944 kg mol<sup>-1</sup> and 1.9, respectively.

#### 2.1.3. Preparation of GR-Based Polymer Composites

Graphene was obtained by Hummers and Offeman<sup>[17]</sup> method via oxidation of graphite, with subsequent ultrasound treatment and reduction (according to the method described in ref.<sup>[18]</sup>). Graphite was oxidised by a treatment with essentially a water-free mixture of concentrated sulfuric acid, sodium nitrate, and potassium permanganate, which took 3 h. The obtained graphite oxide (GO) was exfoliated with the intention to produce GO-sheets using a horn sonicator Sonic Vibracell VC750 with a cylindrical tip of 13 mm end cap diameter, with fixed frequency of 20 ± 2.0 kHz. According to AFM analysis after sonication, most of the graphite oxide sheets exhibit a thickness below 1 nm, corresponding to 2–3 atomic layers, the average surface area of the graphite oxide platelets ranged from 1 to 3 μm<sup>2</sup>.<sup>[16]</sup> The GO-sheets were reduced for 72 h with hydrazine at 120 °C in the presence of a ten-fold excess (wt/wt) of PSS.<sup>[17]</sup> Afterwards the GR covered with PSS was filtered off and dried under vacuum. For the preparation of composites, the GR was dispersed in water by 40 min sonication and mixed with PS or PP latex. The mixture was frozen in liquid nitrogen with subsequent removing of frozen water with a Christ Alpha 2–4 freeze dryer at 0.2 mbar and 20 °C overnight. Bulk samples with various GR loading were obtained by compression molding of composite powder using a Collin Press 300G for 20 min at 180 °C.

## 2.2. Measurements

### 2.2.1. SEM

The composite samples were imaged with a FEI Nova Nanolab 200 (Fei Co.) equipped with a field emission electron source. A secondary electron (SE) detector was used for image acquisition in high vacuum conditions. No additional sample treatment has been performed. Standard acquisition conditions for charge contrast imaging were applied.<sup>[19]</sup> Cross-sectional imaging was performed after freezing samples with liquid nitrogen and subsequent fast cutting.

### 2.2.2. Electrical Conductivity Measurements

Electrical conductivity measurements in DC mode were performed in direction parallel and perpendicular to the sample top surface using 2-probe configuration and a Keithley 2602 system source meter. Conductivity was calculated from the obtained *I/V* characteristics according to the following equation

$$\sigma = \frac{II}{VA} \quad (1)$$

where *V* = applied voltage, *I* = measured current through cross-section *A* between the distance *l*. The distance *l* is the shortest path of current as shown on Figure 1. The numbers for *l* and *A* taken for the calculations are shown in Table 1.

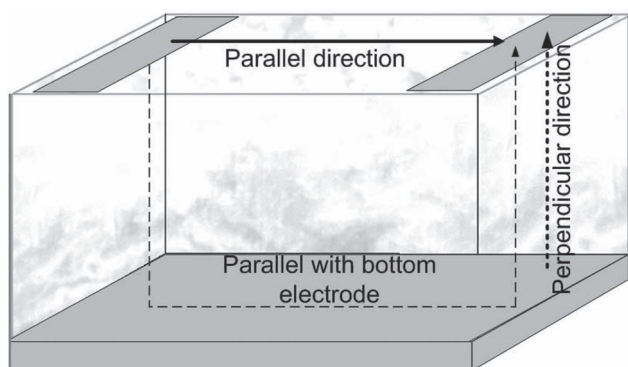


**Figure 1.** Scheme of the DC-measurement setup. The solid line represents the shortest current path in direction parallel with the sample top surface between the two top electrodes without bottom electrode, the dashed line represents the assumed shortest current path between the top electrodes after deposition of an additional bottom electrode; and the pointed line represents the shortest current path in direction through the sample thickness.

As shown in Figure 1, first we have measured the conductivity in direction parallel to the sample top surface between the two gold electrodes with dimensions of  $1 \times 4 \text{ mm}^2$ , thickness of around 100 nm (Figure 1, bold line) and geometry  $l_{\text{par}}$  and  $A_{\text{par}}$  (Table 1). The samples had sizes of  $5 \times 9 \text{ mm}^2$  and varying thickness between 45 and 560  $\mu\text{m}$ . Afterwards, as third electrode, we have sputtered an additional gold film at the bottom side of the samples and have measured the conductivity between the two top electrodes again. Because of the high conductivity of gold, we assume that the shortest path between the top electrodes now goes via the thickness of the sample, which is substantial thinner than the distance between the top electrodes, and the

bottom gold electrode ( $l_{\text{b,el}}$  and  $A_{\text{b,el}}$  in Table 2). In addition, we have measured the conductivity through thickness direction between top and bottom electrodes ( $l_{\text{per}}$  and  $A_{\text{per}}$  in Table 1). All contacts showed linearity of the  $I(V)$  dependency and thus are ohmic. For each sample, the conductivity data represent the average value of 10 consecutive measurements.

### 3. Results and Discussion

#### 3.1. SEM Analysis

Imaging the morphology of purely carbon-based material systems by SEM is difficult mainly because of the lack of contrast. However, particularly for the class of composites, we have investigated in this study, which are composed of a dielectric polymer matrix and conductive carbon allotropic nanofillers, charge contrast imaging has proved to be useful in yielding pronounced contrast between the nanofiller and the matrix with high resolution.<sup>[19,20]</sup> For the case, when a percolating network is formed and the composite shows a certain macroscopic conductivity, high accelerating voltages with incident beam energy of 20 keV can be utilised for imaging the nanofillers without any additional conductive coating covering the sample surface. For such imaging conditions, the primary electrons (PE) generate less SEs in the dielectric polymer matrix than in the GR sheets, which is the main origin for contrast generation between matrix and nanofiller. Moreover, for the high acceleration voltage penetration depths of the PE in carbon is in the order of 2  $\mu\text{m}$ , which has two consequences: on the one hand, information on the network organisation of the GR sheets can be obtained in the volume of the

**Table 1.** Cross-section and taken current path in directions parallel (par), parallel with bottom electrode (b,el) and perpendicular (per) to the sample top surface for composite samples with different graphene loadings.  $l$  and  $A$  are distance and area between the electrodes, respectively.

GR loading [wt%]	$l_{\text{par}}$ [mm]	$l_{\text{b,el}}$ [ $\mu\text{m}$ ]	$l_{\text{per}}$ [ $\mu\text{m}$ ]	$A_{\text{par}}$ [ $\text{mm}^2$ ]	$A_{\text{b,el}}$ [ $\text{mm}^2$ ]	$A_{\text{per}}$ [ $\text{mm}^2$ ]
GR/PS						
0.6	5	310	155	0.62	4	4
0.9	5	180	90	0.36	4	4
1.5	5	90	45	0.18	4	4
2	5	340	170	0.68	4	4
GR/PP						
0.2	5	842	421	1.68	4	4
0.4	5	550	275	1.10	4	4
0.8	5	840	420	1.68	4	4
1.4	5	920	460	1.84	4	4
1.6	5	1120	560	2.24	4	4
2	5	1020	510	2.04	4	4

**Table 2.** As-measured  $I/V$  data taken in directions parallel (par), parallel with bottom electrode and perpendicular (per) to the sample top surface, and corresponding conductivities of the composite samples. Relative error is about 10%.

Gr loading [wt%]	Conductance as measured [S]			Conductivity $\sigma$ (calc.) [ $S\ m^{-1}$ ]		
	Par	Per	Par with bottom electrode	Par	Per	Par with bottom electrode
0.6	$< 3.00 \times 10^{-11}$	$< 3.00 \times 10^{-11}$	$< 3.00 \times 10^{-11}$	$< 2.35 \times 10^{-9}$	$< 1.16 \times 10^{-9}$	$< 2.32 \times 10^{-9}$
0.9	$1.57 \times 10^{-8}$	$4.00 \times 10^{-6}$	$3.30 \times 10^{-6}$	$2.18 \times 10^{-4}$	$8.96 \times 10^{-4}$	$1.41 \times 10^{-4}$
1.5	$6.43 \times 10^{-7}$	$2.27 \times 10^{-3}$	$2.85 \times 10^{-3}$	1.78	1.02	2.57
2	$5.41 \times 10^{-5}$	$1.10 \times 10^{-3}$	$1.31 \times 10^{-3}$	11.92	5.60	4.44
0.2	$2.09 \times 10^{-10}$	$1.54 \times 10^{-9}$	$4.9 \times 10^{-10}$	$6.2 \times 10^{-7}$	$1.62 \times 10^{-7}$	$1.03 \times 10^{-7}$
0.4	$6.42 \times 10^{-10}$	$1.06 \times 10^{-8}$	$6.1 \times 10^{-9}$	$2.92 \times 10^{-6}$	$7.31 \times 10^{-7}$	$8.3 \times 10^{-7}$
0.8	$1.81 \times 10^{-9}$	$1.74 \times 10^{-8}$	$9.26 \times 10^{-9}$	$5.39 \times 10^{-6}$	$1.82 \times 10^{-6}$	$1.94 \times 10^{-6}$
1.4	$1.14 \times 10^{-8}$	$8.15 \times 10^{-8}$	$3.7 \times 10^{-8}$	$3.1 \times 10^{-5}$	$9.37 \times 10^{-6}$	$8.6 \times 10^{-6}$
1.6	$1.17 \times 10^{-6}$	$8.79 \times 10^{-6}$	$4.25 \times 10^{-6}$	$2.62 \times 10^{-3}$	$1.23 \times 10^{-3}$	$1.19 \times 10^{-3}$
2	$1.76 \times 10^{-4}$	$1.37 \times 10^{-3}$	$5.54 \times 10^{-4}$	0.43	0.17	0.14

sample rather than only at the surface,<sup>[21]</sup> and on the other hand, PE can be trapped by GR located in the depths of the sample, which potentially is another origin for contrast generation.<sup>[16,19,20]</sup> As consequence, for the imaging conditions applied in our study, the GR sheets appear bright embedded in the dark polymer matrix.

Figure 2 shows charge contrast images of GR/PS composites with various GR loadings. For loadings below the percolation threshold for forming the conductive GR network, the sample is charged and the image largely shows only artefacts (Figure 2a). When imaging samples with GR loadings above the percolation threshold bright GR particles embedded in the dark polymer matrix become visible. The contrast between GR and matrix becomes more pronounced with increasing the GR loading as more PEs are able to dissipate through more GR platelets, neutralising the negative charging of the dielectric matrix. Brighter GR regions are believed to be closer to the sample surface, while greyish ones are located deeper into the volume.<sup>[20]</sup> For all cases, the GR is represented by platelets, which best can be identified in Figure 2d and e. The GR sheets have sizes of a few micrometres and are randomly oriented; however, because of the contrast mechanism and the platelet shape of GR the eyes catch mainly platelets oriented perpendicular to the primary electron beam, which is parallel to the sample top surface. Figure 2e is a close up at higher magnification in which platelets are highlighted by arrows that are mainly parallel oriented to the primary electron beam. Beside their random orientation, it is obvious that GR does not behave as a stiff platelet but the sheets are bended, wriggled, and sometimes folded.

To gain more evidence on the random orientation of the GR sheets in the PS matrix, we have cross-sectional cut a composite sample with 2 wt% GR loading.

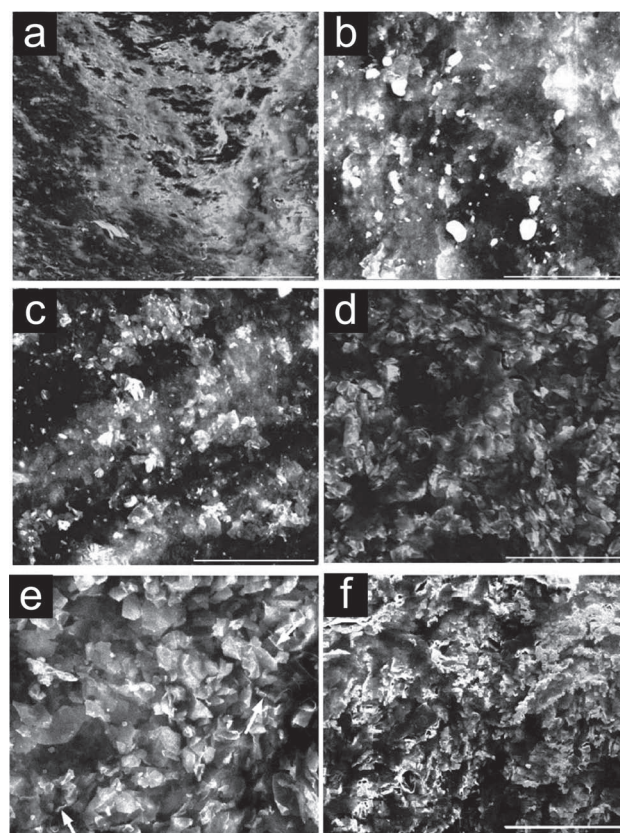


**Figure 2.** SEM charge contrast images of GR/PS composites with different graphene loadings of a) 0.6, b) 0.9, c) 1.5, d)–f) 2 wt%; f) cross-section of the sample. Scale bar for a)–d) is 10  $\mu\text{m}$ , for e) and f) it is 5  $\mu\text{m}$ . The arrows in e) point to graphene sheets laying parallel to the view direction.

Looking from the side, the GR sheets have same dimensions of about few micrometers as already mentioned above, and again appear to be oriented randomly in

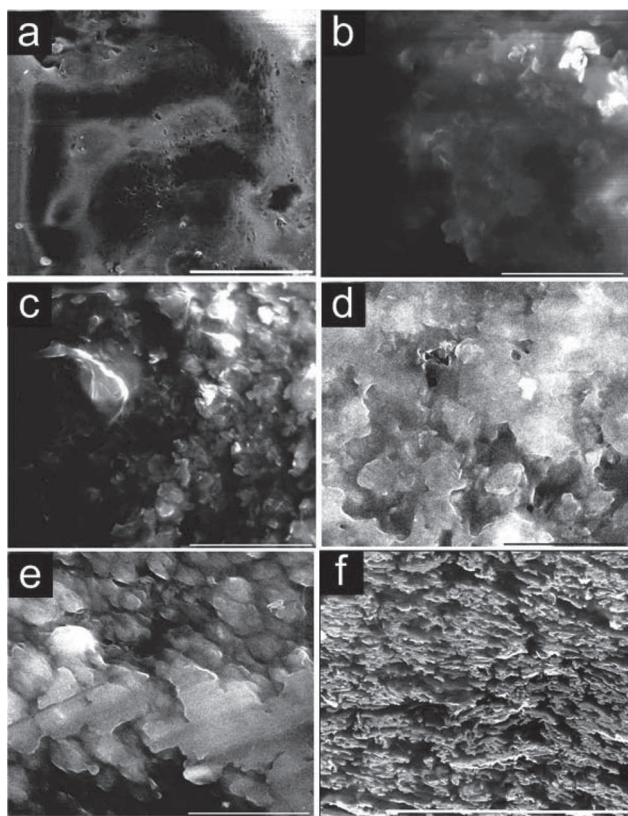


Figure 3. SEM charge contrast images of GR/PP composites with different graphene loadings of a) 0.2 wt%, b) 0.4 wt%, c) 0.8 wt%, d) 1.6 wt%, e) and f) 2 wt%; f) shows the cross-section of the sample. Scale bar is 5  $\mu\text{m}$ .

the matrix with sheets parallel and perpendicular to the direction of the primary electron beam (Figure 2f). From the charging behaviour of the series of samples, we have investigated, we can estimate that the conductivity threshold of the GR/PS composites is in the order of 0.9 wt% GR loading; we will later discuss more details on the percolation behaviour.

Figure 3 represents SEM charge contrast images of GR/PP composites with different GR loadings. For low loadings, the image is dominated by charging artefacts, which indicates that no conductive GR network has been formed in the PP matrix (Figure 3a). For loadings above the conductivity percolation threshold, the bright GR sheets imbedded in the dark PP matrix easily can be identified (Figure 2b–f). However, the contrast of GR in polypropylene appears lower than in PS, probably, due to higher intrinsic conductivity of PP with  $10^{-7} \text{ S m}^{-1}$  compared with  $10^{-9} \text{ S m}^{-1}$  for the PS used in this study. For high loadings and thus the best conditions for charge contrast

imaging, GR sheets clearly can be identified; however, it seems that the GR sheets largely are oriented parallel to the film sample top surface and thus perpendicular to the primary electron beam (Figure 2d and e). Large GR sheets with dimension of several micrometers are visible. Because they are closely stacked and the resolution provided by charge contrast imaging is in the order of tens of nanometres, it seems that the sheets are linked or even fused together. The corresponding cross-sectional side view image confirms that most GR sheets in the GR/PP composite samples are oriented parallel to the sample top surface; we observe mainly sheets that are oriented parallel to the primary electron beam (Figure 3f). From the charging behaviour of the series of samples we have investigated, we can estimate that the conductivity threshold of the GR/PP composites is in the order of 0.4 wt% GR loading.

All composites under investigation are prepared using the identical batch of graphite, oxidation, reduction and dispersion conditions, and following the same general preparation route. However, such significant differences in the organisation of the graphene network might be related to the intrinsic properties of the polymer matrix, which may force different organisation of the network during processing.

In our case, the molecular weight and thus the melt viscosity of the PP is significantly lower than the one of the PS, which certainly influences the melt flow behaviour of the polymer and the embedded GR sheets during compression moulding (Figure 4). For identical processing conditions, polymers with lower melt viscosity will have higher flow velocity during moulding, which may force orientation of the graphene sheets along the flow direction. Of course, corresponding relaxation processes and polymer/GR adhesion have to be considered, too.<sup>[21]</sup> Moreover, in contrast to PS, the PP is a semicrystalline polymer so that its crystallisation behaviour during cooling may influence the organisation of the GR network. Similar to carbon nanotubes,<sup>[22,23]</sup> graphene sheets may nucleate the PP and the ongoing matrix crystallisation disturbs GR network formation.

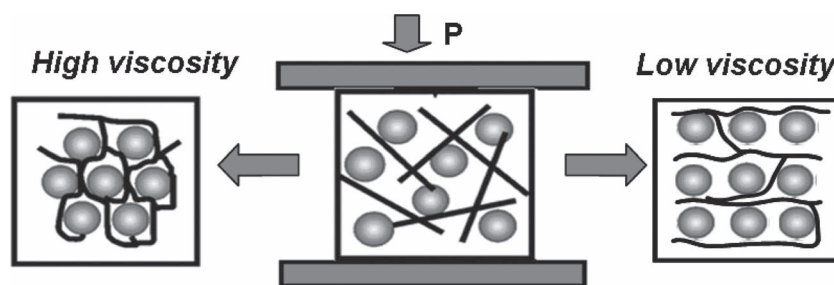
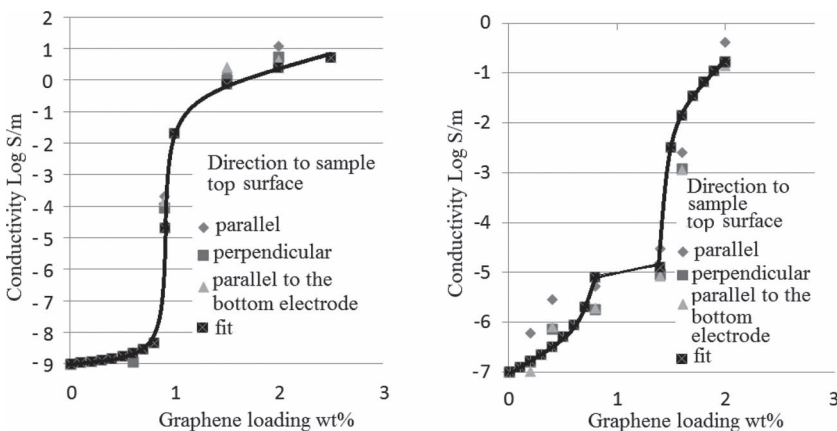


Figure 4. Illustration of the GR organisation in the polymer matrixes potentially caused by the different viscosity and thus flow behaviour of the polymer during compression moulding.



**Figure 5.** Electrical conductivity of graphene-based composites as a function of graphene loading and the polymer matrix used: a) GR/PS, b) GR/PP composites. Values represent an average of 10 measurements for each sample having the standard deviation of about 10%. Solid lines represent theoretical curve fittings using parameters  $t = 0.7$ ,  $s = 2.0$  for GR/PS and  $t = 2.3$ ,  $s = 2.0$  for GR/PP.

### 3.2. Electrical Conductivity Analysis

On the basis of our SEM investigations, the two series of conductive composites seem to have different volume GR network organisation. In the one case, we can identify GR sheets having random orientation in the bulk of the PS matrix and form an isotropic 3D conductive network when loading is above the percolation threshold. On the other hand, for the PP matrix, we have observed GR sheets, which mainly are oriented in direction parallel to the sample top surface, which indicates a 2D network organisation. Because the graphene network is the conductive path inside the dielectric polymer matrix and the only way charges can move along, we can predict that electrical properties of the composites with 3D or 2D graphene networks may differ. To testify this assumption, we have performed a series of electrical conductivity measurements using different setup of electrodes and measuring the conductivity in direction parallel and perpendicular to the samples top surfaces (Figure 1).

When performing conventional 2-point conductivity measurements between the two top electrodes, we find the common conductivity/GR loading behaviour for the PS/GR composites (Table 2 and Figure 5a).<sup>[16]</sup> At low graphene concentrations, the electrical conductivity of the composites remains very close to the conductivity of the pure insulating polymer matrix, because no conductive GR network is formed. The composite exhibits a conductivity percolation threshold at GR loading of around 0.9 wt%. At this concentration, the electrical conductivity increases drastically by five orders of magnitude. At graphene loading of about 2 wt%, the conductivity level reaches  $12 \text{ S m}^{-1}$ . For all conductivity calculations, we have used Equation 1 (see Section 2) with sample parameters as described in Table 1 and Table 2.

Adding the third bottom electrode has resulted in different initial  $I/V$  data-sets when measuring between the top electrodes again (Table 2). Following straightforward considerations, the current always will follow the shortest path with lowest resistance between the electrodes. In the present case, the distance between the two top electrodes is substantial longer than the sample thickness and thus the distance between top and bottom electrode, and resistance of the composite certainly is higher than the resistance of the bottom gold electrode. For the case of an isotropic GR network organisation the current would choose the direct connection between top and bottom electrode, following the bottom electrode and taking shortest path up to the second

top electrode, as it is sketched in Figure 1. Therefore, after correcting the distance  $l$  being now equal to two times the film sample thickness results in similar conductivity as measured without bottom electrode (Table 2) and thus proves the isotropic GR network organisation in the PS matrix. Finally, we have measured the conductivity of the samples between top and bottom electrodes, which again resulted in very similar conductivity values for the entire GR loading range we have investigated. In summary, for each graphene loading electrical conductivities, in all directions are very similar; the overall conductivity data of this series of measurements can be combined and reflects the isotropic 3-D organisation of the graphene sheets in the polymer matrix (Figure 5a).

To further prove the assumption that the GR network in the PS matrix is isotropic, we have applied classical percolation theory and tried to fit our data.<sup>[20]</sup>

$$\sigma = \sigma_f \left( \frac{\phi - \phi_c}{1 - \phi_c} \right)^t, \quad \phi > \phi_c \quad (2)$$

$$\sigma = \sigma_i \left( \frac{\phi_c - \phi}{\phi_c} \right)^{-s}, \quad \phi < \phi_c \quad (3)$$

where  $\sigma$ , conductivity of composite,  $\sigma_f$  and  $\sigma_i$ , electrical conductivities of conductive filler and dielectric matrix,  $\phi$ , filler volume fraction and three fitting parameters, which are  $\phi_c$ , percolation threshold volume fraction,  $t$ ,  $s$ , percolation exponents depended on the lattice dimension.

Parameters for  $\sigma$ ,  $\sigma_f$ ,  $\sigma_i$ ,  $\phi$ , and  $\phi_c$  are taken from experimental data and the fitting is performed by choosing appropriate percolation exponents. Please note that the fundamental mechanism of the nonuniversality of the percolation exponents is still a controversial discussion.<sup>[24]</sup>

The most widely accepted universal values for 3D conductive networks are  $s = 0.7$  and  $t = 2.0$ .<sup>[25]</sup> Following this approach, we have calculated the theoretical conductivity behaviour of the GR/PS nanocomposites using  $t = 0.7$  and  $s = 2.0$  as fitting parameters, which resulted in an excellent fit with the experimental results and thus confirms the 3D isotropic GR network organisation for the GR/PS composites (Figure 5a).

For GR/PP composites, the electrical conductivity behaviour strongly depends on the way it is measured, that is, in direction parallel or perpendicular to the sample top surface and without or with bottom electrode. Figure 5b shows the conductivity/GR loading behaviour as measured for the different setups as described above and in Figure 1. When performing conventional 2-point measurements between the two top electrodes for GR/PP composites the conductivity percolation is at about 0.4 wt% GR loading. However, the overall percolation behaviour seems to be different from the case of GR/PS because instead of a sudden increase of the conductivity by several orders, we observe a rather broad transition range between 0.2 wt% and 2 wt% loading before conductivity reaches a high level of  $0.4 \text{ S m}^{-1}$ . Unfortunately, we had not access to composite samples with higher GR loadings; however, from Figure 5b, we can see that the conductivity did not reach its plateau level so that we assume substantial higher maximum conductivity for higher GR loadings. The broad transition range might be caused by the existence of conductive sub-networks inside the anisotropic network in a not fully percolated system.<sup>[26]</sup> Only for high GR loadings, all sub-networks together create a single conductive network in the bulk of the PP matrix.

The dissimilar percolation behaviour of GR/PP also is reflected in the different conductivity values obtained when measured with and without bottom electrode, and in sample thickness direction and considering the corrected shortest paths, as discussed above (Table 2, Figure 5b). Depending on the measurement setup conductivity can vary by one order of magnitude. It is remarkable that for low GR loadings conductivity between the top electrodes without the bottom electrode always is substantial higher when compared with measurements with bottom electrode and through the thickness of the samples. This behaviour strongly reflects the anisotropic GR network organisation and is in line with our observation of GR sheets predominantly oriented parallel to the film sample surface (Figure 3f).

Finally, we have made an attempt to fit the overall conductivity behaviour of GR/PP with a trend line representing anisotropic 2-D organisation of the graphene sheets (Figure 5b). The fitting is performed according to Equation 2 and 3 with fitting parameters  $t = 2.3$ ,  $s = 2.0$  and percolation threshold of 0.4 wt%, respectively. Again, we would like to note that it is stated that the universal

exponents are nonuniversal for anisotropic systems.<sup>[27,28]</sup> For example in ref.<sup>[27]</sup>, the value of  $t$  was calculated to vary from 1.1 to 1.6 for 2D conductive networks.

## 4. Conclusion

We have studied the conductivity behaviour and volume organisation of polymer composites composed of PS or PP as matrix filled with different loadings of graphene. During sample processing, the different melt flow behaviour of the polymer matrix and the crystallisation of the PP cause predominantly isotropic and nonisotropic orientation of the GR nanofillers in the bulk of GR/PS and GR/PP composites, respectively. SEM charge contrast imaging is able to visualise the GR nanoparticles and shows that for GR/PS composites the GR sheets have no preferred orientation in the bulk of the sample, whereas for GR/PP composites most GR sheets are aligned parallel to the sample top surface.

Corresponding conductivity measurements for different setups in direction parallel and perpendicular to the sample top surface confirm the isotropic 3-D network organisation of GR in GR/PS composites. On the other hand, for GR/PP samples substantial different conductivities are measured for the various measurement setups. Moreover, the broad conductivity percolation transition zone of GR/PP ranging from about 0.2 wt% to 2.0 wt% is another indication for the nonisotropic and predominantly 2-D volume organisation of the GR network in GR/PP composites. Such broad transition zone can be explained by the presence of conductive sub-networks, which gradually connect with each other with increasing GR loading and ultimately form a single network in the bulk of the composite sample. The results obtained in our study demonstrate the importance of understanding the whole composite processing procedure for tuning the electrical and other properties of polymer composites filled with nanoparticles and provide some insights on the bulk network formation of graphene.

**Acknowledgements:** The authors are grateful to Andrew Long, the head of School of Physics and Astronomy, University of Glasgow, for useful discussions. We acknowledge the Ministry of Education and Science of Russia for giving the scholarship for training abroad to Miss Yuliya Syurik (Decree of the Ministry of Education and Science of the Russian Federation N 832 from August 3, 2010).

Received: March 7, 2012; Revised: March 8, 2012; Published online: April 30, 2012; DOI: 10.1002/macp.201200116

**Keywords:** charge contrast SEM; conductive network organization; DC conductivity; graphene composites; morphology

- [1] S. Pande, B. Singh, R. Mathur, T. Dhama, P. Saini, S. Dhawan, *Nanoscale Res. Lett.* **2009**, *4*, 327.
- [2] S.-H. Park, P. T. Theilmann, P. M. Asbeck, P. R. Bandaru, *IEEE Trans. Nanotechnol.* **2011**, *9*, 464.
- [3] S. Stankovich, D. A. Dikin, G. H. B. Dommett, K. M. Kohlhaas, E. J. Zimmey, E. A. Stach, R. D. Piner, S. T. Nguyen, R. S. Ruoff, *Nature* **2006**, *442*, 282.
- [4] F. Du, R. C. Scogna, W. Zhou, S. Brand, J. E. Fischer, K. I. Winey, *Macromolecules* **2004**, *37*, 9048.
- [5] K. Lu, N. Grossiord, C. Koning, H. Miltner, *Polymer* **2008**, *41*, 8081.
- [6] A. K. Geim, K. S. Novoselov, *Nat. Mater.* **2007**, *6*, 183.
- [7] N. Grossiord, J. Loos, O. Regev, C. E. Koning, *Chem. Mater.* **2006**, *18*, 1089.
- [8] N. Grossiord, J. Loos, C. E. Koning, *J. Mater. Chem.* **2005**, *15*, 2349.
- [9] L. F. Francis, J. C. Grunlan, J. K. Sun, W. W. Gerberich, *Colloids Surf. A* **2007**, *311*, 48.
- [10] Y. S. Kim, J. B. Wright, J. C. Grunlan, *Polymer* **2008**, *49*, 570.
- [11] S. Stankovich, R. D. Piner, S. T. Nguyen, R. S. Ruoff, *Carbon* **2006**, *44*, 3342.
- [12] B. McCarthy, J. N. Coleman, R. Czerw, A. B. Dalton, M. in het Panhuis, A. Maiti, A. Drury, P. Bernier, J. B. Nagy, B. Lahr, H. J. Byrne, D. L. Carroll, W. J. Blau, *J. Phys. Chem. B* **2002**, *106*, 2210.
- [13] K. S. Kim, Y. Zhao, H. Jang, S. Y. Lee, J. M. Kim, J. H. Ahn, P. Kim, J. Y. Choi, B. H. Hong, *Nature* **2009**, *457*, 706.
- [14] G. Eda, G. Fanchini, M. Chhowalla, *Nat. Nanotechnol.* **2008**, *3*, 270.
- [15] T. Sekitani, Y. Noguchi, K. Hata, T. Fukushima, T. Aida, T. Somey, *Science* **2008**, *321*, 1468.
- [16] E. Tkalya, M. Ghislandi, A. Alekseev, C. Koning, J. Loos, *J. Mater. Chem.* **2010**, *20*, 3035.
- [17] W. S. Hummers, R. E. Offeman, *J. Am. Chem. Soc.* **1958**, *80*, 1339.
- [18] S. Stankovich, R. D. Piner, X. Chen, N. Wu, S. T. Nguyen, R. S. Ruoff, *J. Mater. Chem.* **2006**, *16*, 155.
- [19] J. Loos, A. Alexeev, N. Grossiord, C. E. Koning, O. Regev, *Ultra-microscopy* **2005**, *104*, 160.
- [20] W. Li, S. T. Buschhorn, K. Schulte, W. Bauhofer, *Carbon* **2011**, *49*, 1955.
- [21] U. A. Handge, P. Pötschke, *Rheologica Acta* **2007**, *46*, 889.
- [22] H. E. Miltner, N. Grossiord, K. Lu, J. Loos, C. E. Koning, B. Van Mele, *Macromolecules* **2008**, *41*, 5753.
- [23] K. Lu, N. Grossiord, C. E. Koning, H. E. Miltner, B. van Mele, J. Loos, *Macromolecules* **2008**, *41*, 8081.
- [24] W.-Z. Cai, S.-T. Tu, J.-M. Gong, *J. Composite Mater.* **2006**, *40*, 2131.
- [25] H. D. Wagner, O. Lourie, Y. Feldman, R. Tenne, *Appl. Phys. Lett.* **1998**, *72*, 188.
- [26] A. Alekseev, A. Efimov, K. Lu, J. Loos, *Adv. Mater.* **2009**, *21*, 4915.
- [27] K. S. Mendelson, F. G. Karioris, *J. Phys. C* **1980**, *13*, 6197.
- [28] S. Yoon, S. I. Lee, *Physica B* **1990**, *167*, 133.